Abstracts of ISAFM2017

The 8th International Symposium on Advanced Functional Materials
between Yokohama National University
and Changwon National University

February 20 - 22, 2017

Yokohama National University

Education and Culture Hall
Yokohama, Japan

Organized by

Yokohama National University, Department of Solid State Materials and Eng., Japan
Changwon National University, Department of Nano and Advanced Materials Eng., Korea

Supported by

Yokohama National University, Japan
Changwon National University, Korea

YNU
YOKOHAMA National University

CHANGWON NATIONAL UNIVERSITY

List of participants

Title	Name	Japanese reading	Affiliation
faculty	Hiroshi Fukutomi	福富 洋志	YNU, JAPAN
faculty	Osamu Umezawa	梅澤 修	YNU, JAPAN
faculty	Kohki Mukai	向井 剛輝	YNU, JAPAN
faculty	Junichi Tatami	多々見 純一	YNU, JAPAN
faculty	Shoichi Hirosawa	廣澤 渉一	YNU, JAPAN
faculty	Wataru Nakao	中尾 航	YNU, JAPAN
faculty	Mahoto Takeda	竹田 真帆人	YNU, JAPAN
faculty	Makoto Hasegawa	長谷川 誠	YNU, JAPAN
faculty	Hiroshi Nakatsugawa	中津川 博	YNU, JAPAN
faculty	Tomoyoshi Maeno	前野 智美	YNU, JAPAN
faculty	Norimitsu Koga	古賀 紀光	YNU, JAPAN
faculty	Hideaki Iwaoka	岩岡 秀明	YNU, JAPAN
faculty	Kazuto Okayasu	岡安 和人	YNU, JAPAN
student	Shosuke Kogo	古後 翔佑	YNU, JAPAN
student	Fumimasa Suetsugu	末続 文正	YNU, JAPAN
student	Kotatsu Hirata	平田 弘達	YNU, JAPAN
student	Ayuka Matsugami	松上 歩加	YNU, JAPAN
student	JangWon Lee	ジャンウォン リ	YNU, JAPAN
student	Weibo Li	ウイボ リ	YNU, JAPAN
student	Takayuki Yamashita	山下 享介	YNU, JAPAN
student	Jun Seop Kim	金 俊燮	YNU, JAPAN
student	Natsuko Kimura	木村 奈津子	YNU, JAPAN
student	Takahiro Yamazaki	山崎 貴大	YNU, JAPAN
student	Shuntaro Tsukamoto	塚本 俊太郎	YNU, JAPAN
student	Yusaku Yasumori	安盛 雄作	YNU, JAPAN

Title	Name	Japanese reading	Affiliation
faculty	Chan Gyu Lee	チャン ギュ イ	CNU, KOREA
faculty	Dong Sik Bae	ドン シク べ	CNU, KOREA
faculty	Hyun Uk Hong	ヒョン ウク ホン	CNU, KOREA
faculty	Hee Kyu Choi	ヒ ギュ チェ	CNU, KOREA
faculty	Mathieu Terner	マチュー ターナー	CNU, KOREA
faculty	Sun Woog Kim	ソン ウク キム	Sejong Uni., KOREA
student	Jeong Hun Son	ジョン フン ソン	CNU, KOREA
student	Won Joon Lee	ウォン ジュン イ	CNU, KOREA
student	Hyeon Tae Im	ヒョン テ イム	CNU, KOREA
student	Dong Gyu Lee	ドン ギュ イ	CNU, KOREA
student	Yeon Bin Choi	ヨン ビン チェ	CNU, KOREA
student	Ji Young Ock	ジ ヨン オク	CNU, KOREA
student	Han Ul Choi	ハン ウル チェ	CNU, KOREA
student	Hyun Mi Lee	ヒョン ミ イ	CNU, KOREA
student	Kyeong Yong Shin	ギョン ヨン シン	CNU, KOREA
student	Chi Won Kim	チ ウォン キム	CNU, KOREA

ISAFM2017

The 8th International Symposium on Advanced Functional Materials
between Yokohama National University
and Changwon National University

February 20 - 22, 2017

Yokohama National University

Education and Culture Hall
Yokohama, Japan

Organized by

Yokohama National University, Department of Solid State Materials and Eng., Japan
Changwon National University, Department of Nano and Advanced Materials Eng., Korea

Supported by

Yokohama National University, Japan
Changwon National University, Korea

Organizing Committee

General Chairs

Prof. Shoichi Hirosawa, Yokohama National University, JAPAN, hirosawa-shoichi-mc@ynu.ac.jp

Prof. Mahoto Takeda, Yokohama National University, JAPAN, takeda-mahoto-mk@ynu.ac.jp

Prof. Chan Gyu Lee, Changwon National University, KOREA, chglee@changwon.ac.kr

Prof. Dong Sik Bae, Changwon National University, KOREA, dsbae7@changwon.ac.kr

Academic Committee Chairs

Prof. Hiroshi Fukutomi, Yokohama National University, JAPAN, fukutomi-hiroshi-pk@ynu.jp

Prof. Osamu Umezawa, Yokohama National University, JAPAN, umezawa-osamu-fv@ynu.ac.jp

Prof. Kohki Mukai, Yokohama National University, JAPAN, mukai-kohki-cv@ynu.ac.jp

Prof. Junichi Tatami, Yokohama National University, JAPAN, tatami-junichi-xv@ynu.ac.jp

Prof. Wataru Nakao, Yokohama National University, JAPAN, nakao-wataru-hy@ynu.ac.jp

Prof. Hiroshi Nakatsugawa, Yokohama National University, JAPAN, nakatsugawa-hiroshi-dx@ynu.ac.jp

Prof. Makoto Hasegawa, Yokohama National University, JAPAN, hasegawa-makoto-zy@ynu.ac.jp

Prof. Tomoyoshi Maeno, Yokohama National University, JAPAN, maeno-tomoyoshi-yf@ynu.ac.jp

Prof. Norimitsu Koga, Yokohama National University, JAPAN, koga-norimitsu-sx@ynu.ac.jp

Prof. Hideaki Iwaoka, Yokohama National University, JAPAN, iwaoka-hideaki-xd@ynu.ac.jp

Mr. Kazuto Okayasu, Yokohama National University, JAPAN, okayasu-kazuto-kx@ynu.ac.jp

Prof. Hyun Uk Hong, Changwon National University, KOREA, huhong@changwon.ac.kr

Prof. Hee Kyu Choi, Changwon National University, KOREA, hkchoi99@changwon.ac.kr

Prof. Mathieu Terner, Changwon National University, KOREA, mathieu@changwon.ac.kr

Prof. Sun Woog Kim, Sejong University, KOREA, skim80@sejong.ac.kr

Preface

Materials science and engineering is constructed by interdisciplinary fields, and encompasses complete knowledge for materials bridging the basic and applied sciences. The International Symposium on Advanced Functional Materials, ISAFM, was launched in 2009 at Changwon, Korea, to offer a valuable opportunity for exchanging knowledge and scientific idea of researchers and students at both of Yokohama National University (YNU) and Changwon National University (CNU). The ISAFM 2017 held in 20-22 February, 2017 at Yokohama, Japan, is the 8th YNU/CNU symposium, and 16 papers concerning metallic materials, energy conversion materials, nano-materials and nano technology are included together with four plenary lectures as invited presentations. The symposium also aims to make friendship among participants, and to encourage international collaboration and exchange program between both national universities.

I would like to express sincere thanks and gratitude to my colleagues who prepared all the ISFAM events, in particular, Prof. M. Takeda. I wish all participants to have a pleasant stay in Yokohama, and I hope that the ISAFM 2017 will remain in their memory as an enjoyable and scientifically important experience.

21 February, 2017

Shoichi HIROSAWA
Yokohama National University

General Information

Welcome reception

- **Welcome reception will be held on February 20 in the Cafeteria Ⅱ COOP, 18:00-19:30.**

Registration fee

- **Registration desk will operate at 8:45-9:15 February 21 in the Education and Culture Hall.**

> **Japanese faculty: 33,000JPY**
>
> **Japanese student: 22,000JPY**
>
> **Korean faculty: 10,000JPY (On site by cash)**
>
> **Korean student: 10,000JPY (On site by cash)**

Lunch

- **Lunch will be held on February 21 in Cafeteria Ⅰ (Renga Kan), 12:00-13:15**

Banquet

- **Banquet will be held on February 21**

  in CRUISE-CRUISE YOKOHAMA (Sky Building 27F),

  19:00-21:30

Accommodation

- **Hotel Yokohama Camelot Japan**

Language

- **ENGLISH will be the official language during ISAFM2017.**

Campus Map of Yokohama National University

Hijirigaoka

Kamadaijuutaku-dai1

Bus Stop: Kokudai-nishi

West Gate

Kokudai-nishi

Kamadai juutaku-dai2

Staff Quarters

Cafeteria II COOP (Welcome reception)

Water Tower

South Gate

Kokudai-minamimon

Bus Stop: Daigakukaikan-mae

South Side Gate

South Area

South of the main street is indicated by S-Area

Cafeteria I Renga Kan (Lunch)

Education and Culture Hall (Registration and Symposium)

Yokohama-shindo

Tennis Court

Baseball Ground

Swimming Pool

Futsal Field

Football Field

Adjustment Pool

Athletics Field

North Gate

Adjustment Pool

Central Park

Main Street

Central Library

CentralPark

Kokudai-kita

Kokudai-Chuo Kokudai-Chuo

East Side Gate

Small Sports Ground

Nursery

Daigakukaikan-mae

Multi-purpose Sports Ground

Main Gate

Yokohama-kokuritsu-daigaku-seimon-mae

Okazawa-cho

North Area

North of the main street is indicated by N-Area

Legend

🍴 Cafeteria and Lunch Box Stand
🧑 Student/ Educational Affairs Section
🖥 PC Room
📄 Certificate Issuing Machine
🚲 Autobike Parking
Ⓟ Parking Lot
⚲ Bus Stop
🔵 Bus Stop (inside campus)

N10 N9 N8 N7 N6 N5 N4 N3 N2 N1
S8 S9 S7 S6 S5 S4 S3 S2 S1 S0

- 5 -

By Airplane

- Narita Airport → Narita Express (90 min.) → Yokohama Station
- Narita Airport →　Airport Limousine Bus (120 min.)　→ YCAT*
- Haneda Airport →　Keihinkyuko Line (20 min.) → Yokohama Station
- Haneda Airport → Keikyu Bus (30 min.) → YCAT*

YCAT(Yokohama City Air Terminal) is located in the SKY Building behind the east exit of Yokohama Station.

By Bullet Train

- If you get off at Tokyo Station → Take any of the JR lines (The ride time Tokaido Line: 30 min., Yokosuka Line: 35 min., Keihin Tohoku Line: 45 min.) →　Get off at Yokohama Station
- If you get off at Shin-Yokohama Station → Take the Yokohama City Subway (About a 10 min. ride) → Get off at Mitsuzawa-kamicho Station

By Train

The Nearest Station: [Yokohama Municipal Subway] Mitsuzawa-kamicho Station → About a 16 min. walk
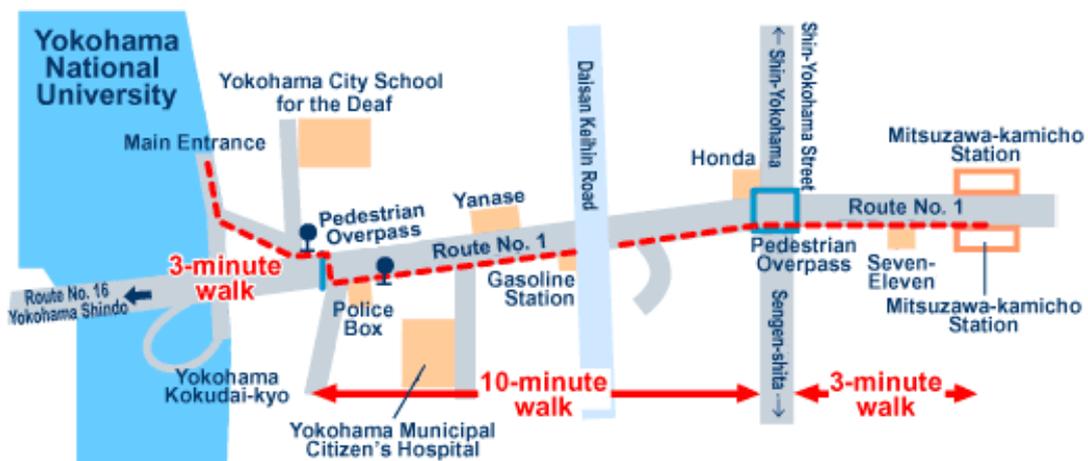
By Taxi

It takes 15 minutes from the West Exit of Yokohama Station.

By Bus

It takes 15-20 minutes from the bus terminal at the West Exit of Yokohama Station to YNU.

Bus Stop at the West Exit of Yokohama Station
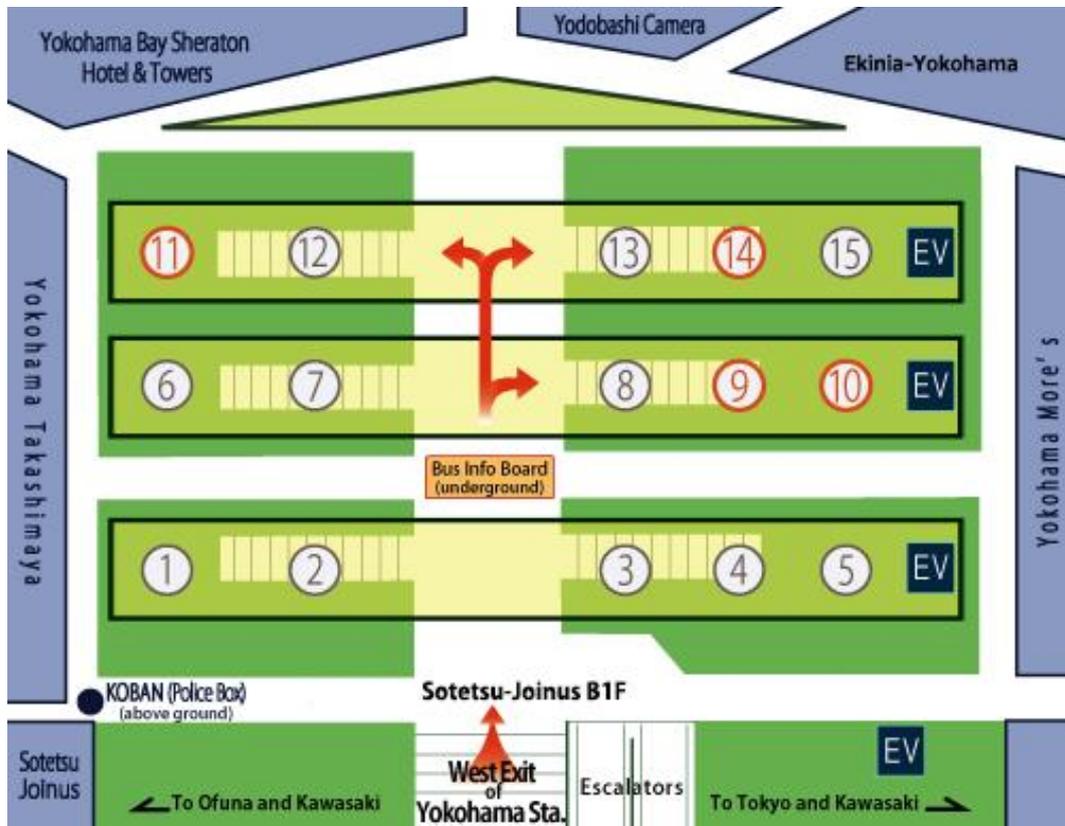
Sotetsu Bus		
Platform		10
Bus No. & Destination		#Hama-10 for Yokohama Sta. West Exit
Bus Stops to get off	**OFF-Campus**	Yokohama-shindo or Okazawa-cho
	ON-Campus weekdays only	Bus Timetable 📄 See the Map 📄

Platform		10
Bus No. & Destination		#Hama-5 for Yokohama Sta. West Exit via Kotsu Saibansho
Bus Stops to get off	**OFF-Campus**	Okazawa-cho

Platform		9
Bus No. & Destination		#Hama-11 for Kamadaijuutaku-dai-san(3) or Kamihoshikawa
Bus Stops to get off	**OFF-Campus**	Kamadaijuutaku-dai-ichi(1) and Hijirigaoka

Program

Monday, February 20, 2017

■ **Welcome reception, 18:00-19:30**

・ **Cafeteria Ⅱ COOP**

Tuesday, February 21, 2017

■ **Registration, 8:45-9:15**

・ **Education and Culture Hall**

■ **Opening Address, 9:15-9:25**

・ **9:15-9:18 President of YNU: Prof. Yuichi Hasebe (planned) (YNU, JAPAN)**

・ **9:18-9:21 Prof. Chan Gyu Lee (CNU, KOREA)**

・ **9:21-9:25 Prof. Shoichi Hirosawa (YNU, JAPAN)**

■ **Oral Session 1：Chairman, Prof. Wataru Nakao (YNU, JAPAN)**

9:25-10:35 (Lecture; 10min and Plenary lecture; 20min)

・ **9:25-9:50 Plenary lecture01: Prof. Sun Woog Kim (Sejong University, KOREA)**
  ➢ Design of Novel Oxide Phosphor Exhibiting Long Wavelength Emission

・ **9:50-10:05 lecture001 : Won Joon Lee (CNU, KOREA)**
  ➢ Fabrication and Characterization of Gd doped CeO_2 by Solvothermal process

・ **10:05-10:20 lecture002: Ayuka Matsugami (YNU, JAPAN)**
  ➢ Low wear rate of AlN ceramics based on tribo-chemical reactions

・ **10:20-10:35 lecture003: Ji Young Ock (CNU, KOREA)**
  ➢ A simple way to synthesize $K_3V_5O_{14}$ red inorganic pigment by a WASSR method

■ Oral Session 2 : Chairman, Prof. Hee Kyu Choi (CNU, KOREA)

10:50-12:00 (Lecture; 10min and Plenary lecture; 20min)

- **10:50-11:15 Plenary lecture02: Prof. Tomoyoshi Maeno (YNU, JAPAN)**
  - Improvement of uniformity in hardness distribution of die-quenched products in hot stamping using rapid resistance heating

- **11:15-11:30 lecture004: Kyeong Yong Shin (CNU, KOREA)**
  - Effect of Heat Treatment on Microstructure Evolution and the Tensile Properties of Haynes 282 Superalloy

- **11:30-11:45 lecture005: Weibo Li (YNU, JAPAN)**
  - A Review of subsurface crack initiation models in high-cycle fatigue for titanium alloys

- **11:45-12:00 lecture006: Hyeon Tae Im (CNU, KOREA)**
  - Fabrication and Characterization of $Ag-SiO_2$ / Inorganic Antimicrobial coating agent

■ Lunch, 12:00-13:15

- **Cafeteria Ⅰ (Renga Kan)**

■ Oral Session 3 : Chairman, Prof. Makoto Hasegawa (YNU, JAPAN)

13:15-14:25 (Lecture; 10min and Plenary lecture; 20min)

- **13:15-13:40 Plenary lecture03: Prof. Mathieu Terner (CNU, KOREA)**
  - The prospect of Metal Additive Manufacturing towards performance and innovations

- **13:40-13:55 lecture007: Takayuki Yamashita (YNU, JAPAN)**
  - The stability of retained austenite and transformation behaviour in TRIP steels at low temperature

- **13:55-14:10 lecture008: Chi Won Kim (CNU, KOREA)**
  - Atom probe study of the precipitation of κ-carbide with Si addition and dislocation behavior in a cast FeMnAlC lightweight steel

- **14:10-14:25 lecture009: Shosuke Kogo (YNU, JAPAN)**
  - Thermodynamic Assessment and Determination of Phase Diagram Including Spinodal Lines in Al-Mg Alloy

■ Oral Session 4 : Chairman, Prof. Hyun Uk Hong (CNU, KOREA)

14:40-15:50 (Lecture; 10min and Plenary lecture; 20min)

・ **14:40-15:05 Plenary lecture04: Prof. Norimitsu Koga (YNU, JAPAN)**
  ➢ Analysis of Strain distribution in deformed materials by digital image correlation

・ **15:05-15:20 lecture010: Dong Gyu Lee (CNU, KOREA)**
  ➢ Morphology of Aluminium (Al 3003) Chemical Etching for Insert Molding

・ **15:20-15:35 lecture011: Kotatsu Hirata (YNU, JAPAN)**
  ➢ Microstructural Change of Thermal Barrier Coatings Deposited on TiAl Alloy

・ **15:35-15:50 lecture012: Yeon Bin Choi (CNU, KOREA)**
  ➢ Synthesis and Characterization of $K_2Ti_6O_{13}$ Whisker by Flux method

■ Oral Session 5 : Chairman, Prof. Dong Sik Bae (CNU, KOREA)

16:05-17:05 (Lecture; 10min and Plenary lecture; 20min)

・ **16:05-16:20 lecture013: Han Ul Choi (CNU, KOREA)**
  ➢ Effect of Preparation Methods on the Electrochemical Performance of All-solid-state Li-S battery

・ **16:20-16:35 lecture014: Fumimasa Suetsugu (YNU, JAPAN)**
  ➢ Control of Electron Coupled State in Superlattice of PbS Quantum Dots by Replacing Ligands

・ **16:35-16:50 lecture015: Hyun Mi Lee (CNU, KOREA)**
  ➢ The effect of hydrogen sulfide(H_2S) on sulfur poisoning of nickel-yttria stabilized zirconia(Ni-YSZ) anode supported solid oxide fuel cells

・ **16:50-17:05 lecture016: Jang Won Lee (YNU, JAPAN)**
  ➢ Competition Behavior between defect propagation and self-healing under high temperature creep in Fiber-reinforced self-healing ceramics

■ Closing remark, 17:05-17:15

・ **Prof. Hiroshi Fukutomi (YNU, JAPAN)**

■ Banquet, 19:00-21:30

・ **CRUISE-CRUISE YOKOHAMA (Sky building 27F)**
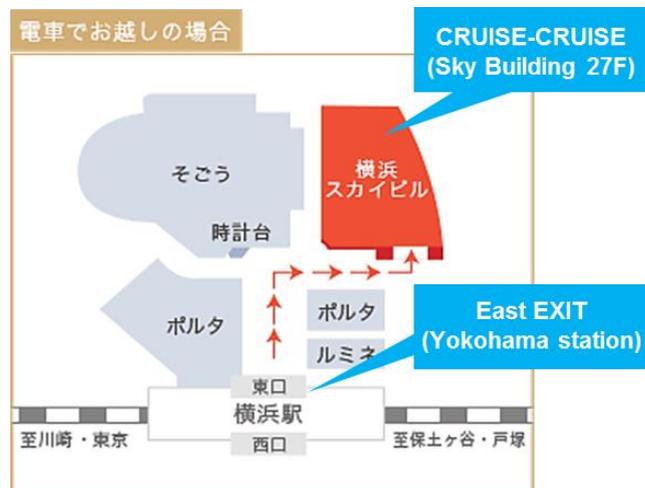
Wednesday, February 22, 2017

■ Lab Tour, 9:00-10:30

■ Departure

Abstracts

Design of Novel Oxide Phosphor Exhibiting Long Wavelength Emission

Sun Woog Kim[1†], Takuya Hasegawa[2], Kenji Toda[3], Mineo Sato[3]

Sejong University[1], Kochi University[2], Niigata University[3]

209 Neungdong-ro, Gwangjin-gu, Seoul 05006, Republic of Korea[1], 200 Otsu, Monobe, Nankoku City, Koch 783-8502, Japan[2], 8050 Ikarashi 2-nocho, Niigata 950-2181, Japan[3]

TEL: +81-2-6935-2444 E-mail:skim80@sejong.ac.kr

Typical white LEDs composed of blue light excitable green- and red-emission phosphors and blue LED chip. As a red-emission phosphor, Eu^{2+}-activated nitrides or Mn^{4+}-doped fluoride phosphors have been mainly used, however, these phosphors require special furnace or atmosphere to synthesize a single phase materials. The development of novel red-emission phosphors, which can be easily synthesized in normal processing, is extremely important in white LEDs application. In addition, blue light excitable long wavelength emission phosphors have been recently investigated as a spectral converter to enhance the energy conversion efficiency of silicon solar cells. Therefore, the investigations have been devoted to search for novel approach to develop novel long wavelength emission phosphor for use in white LEDs and silicon solar cells as a spectral converter. In this study, we proposed the further approach to develop novel long wavelength emission phosphors and presented the luminescence properties of the novel phosphors developed using further approach.

Fabrication and Characterization of Gd doped CeO₂ by Solvothermal process

Won-Joon Lee, Jeong-Hun Son, Dong-Sik Bae[†]

Department of Advanced Materials Engineering, Changwon National University
*Department of Convergence Materials Science and Engineering, Changwon National Univ., 20
Changwondaehak-ro Uichang-gu Changwon-si, Gyeongsangnam-do 641-773 KOREA.
TEL: +82-55-275-5475   E-mail: dsbae7@changwon.ac.kr*

Abstract Gd doped CeO_2 nanopowders were prepared under low temperature and high pressure conditions by solvothermal process from metal nitrates with aqueous ammonium hydroxide. Gd doped Ceria nanopowders were obtained by a reaction at the temperature range of 120℃~180℃ for 2~6h. The average size and size distribution of the synthesized particles were around 5~10nm and spherical, respec1tively. The specific surface area of the synthesized Gd doped CeO_2 particles above 130m²/g. The XRD diffraction pattern shows that the synthesized powders were crystalline. This study has shown that the synthesis of Gd doped CeO_2 nanopowders is possible under solvothermal conditions in distilled water/ethanol solution. The effects of synthesis parameters, such as the solvent ratio of starting solution, pH of starting solution, reaction temperature and time, are discussed.

Experimental Cerium acetate and Gadolinium nitrate hexahydrate (3mol %) are mixed in distilled water and ethanol. Using ammonium hydroxide to a pH in the range 7~11. The precipitate was washed with distilled water and then Solvothermal process for 2~6h at 120~180℃ to convert to Gd doped CeO_2. After performing Solvothermal process, washing 5 times for 10 min with ethanol and dried at 100℃ for 24h in air.

Results and Discussion The crystal shape and size of synthesized Gd doped ceria were controlled through reaction temperature and ratio of ethanol and water. The synthesized Gd doped ceria nanopowders was crystallinity and sure to include crystal structure of ceria on Gd as matrix at X-ray Diffraction analysis. The particle size was calculated using a Scherer equation and it was 3~6nm. The shapes of synthesized Gd doped ceria were spherical at Field Emission Scanning Electron Microscopy. The specific surface area of Gd doped ceria were characterized by BET that around 110~130m²/g.
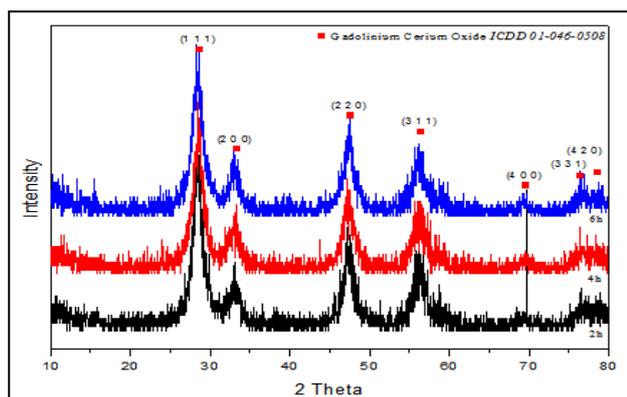
Fig.1 XRD diffraction patterns of Gd doped CeO₂.
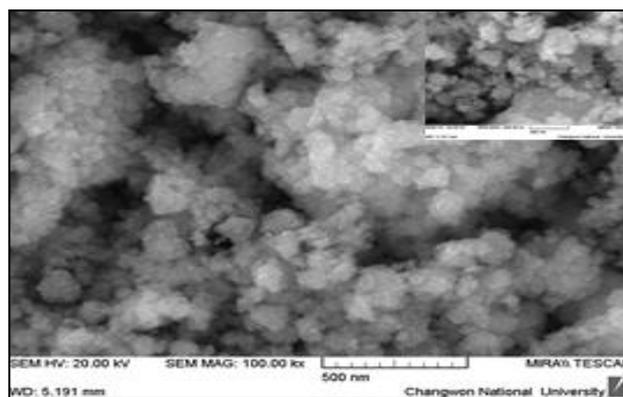
Fig.2 FESEM image of Gd doped CeO₂.

References
1) T. S. Zhang, J. Ma, L. B. Kong, P. Hing and J. A. Kilner, "Preparation and mechanical properties of dense $Ce_{0.8}Gd_{0.2}O_{2-\delta}$ ceramics", Solid State Ionics. 167 (2004) 191.
2) G Dell'Agli, L Spiridigliozzi, A Marocco, G. Accardo, C. Ferone and R. Cioffi, "Effect of the mineralizer solution in the hydrothermal synthesis of gadolinium-doped (10% mol Gd) ceria nanopowders.", J Appl Biomater Funct Mater. 14(2) (2016) e189.

Low wear rate of AlN ceramics based on tribo-chemical reactions

Ayuka Matsugami[1], Junichi Tatami[1], Motoyuki Iijima[1], Hideyuki Ohguni[2]

[1]Yokohama National University, [2]Sumitomo Electric Industries, Ltd.
[1]*Yokohama, Kanagawa 240-8501, Japan,* [2]*Itami,Hyogo 664-0016, Japan*
TEL: +81-45-339-3959   E-mail: tatami-junichi-xv@ynu.ac.jp

Abstract Wear behavior of material depends on the properties of the material. According to the wear map by Adachi (1995)[1], it suggests that a threshold of the mild wear region and the severe wear region be lower if soft compounds are on worn surface. Moreover, the tribo-chemical reaction could be incited on the surface of materials by friction or wear depending on surrounding atmosphere. For example, it is said that aluminum nitride, AlN, forms oxide and hydroxide layer during ball milling. It should be easy to be incited tribo-chemical reaction. Therefore, in this study, we aim to achieve low wear rate of AlN ceramics based on tribo-chemical reactions.

Experimental AlN ceramics were fabricated using the AlN powder with 0.6 mol% of the Y_2O_3 powder. The green bodies of the powder mixture were fired at 1850℃ for 2 h in 0.6 MPa N_2. After polishing the surface of the AlN ceramics, ball-on-disk test of the specimens was performed under 20% relative humidity (low humidity air), over 50% relative humidity (high humidity air) and in CO_2 flow under 20% relative humidity (CO_2 flow air). After the wear test, their cross section profiles were estimated by lasermicroscope to calculate their wear volume and their worn surfaces were observed by SEM and EDS.

Results and Discussion Fig.1 shows wear volume of AlN ceramics under different atmosphere and specific wear rate. We discover that the wear behavior of AlN ceramics strongly depends on the humidity. From the observation of the worn surfaces by SEM, we found the differences depending on the atmosphere. After the test in the low humidity air, AlN grains fell off because the intergranular fracture is dominant. (Fig.2(a))On the other hand, after the test in the high humidity air, the worn surface is very smooth because tribo-chemical reactions are dominant. (Fig.2(b)) To promote the reactions, the other ball on disk test was performed in CO_2 flow air. In this case, the lowest wear rate of 2.6×10^{-10} mm²/N was achieved. The low wear rate resulted from the soft layer formed by tribo-chemical reactions on the worn surface, which prevents from thermal shock.(Fig.3)
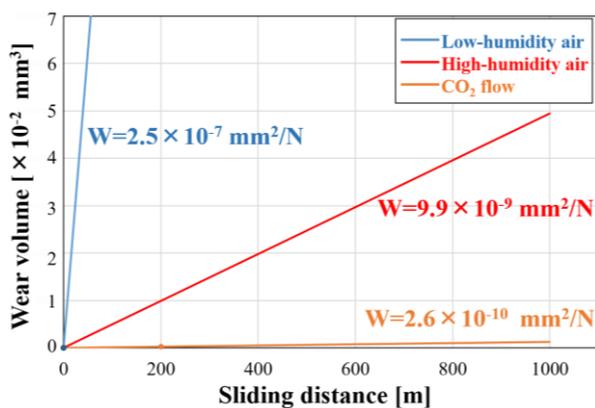
Fig.1 Wear volume of AlN ceramics under different atmosphere and specific wear rate
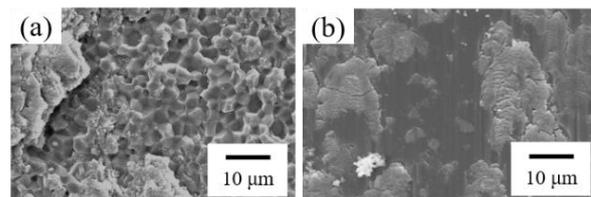
Fig.2 SEM images of worn surfaces of AlN ceramics after ball-on-disk test in (a) low humidity air and (b)high humidity air.
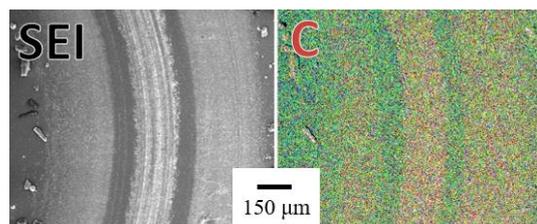
Fig.3 SEM image and EDS image of worn surface of AlN

Reference
1) K. Adachi, et al., *Wear Map of Ceramics*, Wear, 209-204, 291-301 (1997)

A simple way to synthesize $K_3V_5O_{14}$ red inorganic pigment by a WASSR method

Ji-Young Ock[1], Sun-Woog Kim[2†] and Dong-Sik Bae[1†]

Changwon National University[1], Sejong University[2]

20, Changwondaehak-ro, Uichang-gu, Changwon-si, Gyeongsangnam-do, Republic of Korea[1], 209, Neungdong-ro, Gwangjin-gu, Seoul, Republic of Korea[2]

TEL: +81-55-275-5475   E-mail:dsbae7@changwon.ac.kr[1], E-mail:skim80@sejong.ac.kr[2]

Abstract $K_3V_5O_{14}$ inorganic red pigment was synthesized by a water assisted solid state reaction (WASSR) method, which is simple low temperature synthesis method. The $K_3V_5O_{14}$ pigment showed a strong broad optical absorption in the green light region owing to the charge transfer (CT) transition from the O^{2-} 2p orbital to V^{5+} 3d orbital in the VO_n (n = 4 and 5) polyhedral. At an excitation wavelength of 365 nm, this pigment exhibited a broad red emission with a peak at 613.2 nm. The $K_3V_5O_{14}$ pigment showed a bright-vivid red body color and the L*, a* and b* values were 52.1, 35.75 and 19.06, respectively.

Experimental K_2CO_3 and V_2O_5 was mixed for 1 min using a agate mortar, and then the mixture was placed into a teflon bottle and stored at 100 ºC for 24 h in oven. The obtained sample was heated at 400 ºC for 6 h to obtain a single phase with high crystallinity.

Results and Discussion Upon the monitoring wavelength at 365 nm, $K_3V_5O_{14}$ pigment showed an asymmetric broad emission band due to $^3T_2 \rightarrow {}^1A_1$ and $^3T_1 \rightarrow {}^1A_1$ transition of the $[VO_4]^{3-}$ group (Fig. 1). From the UV-vis diffuse reflectance spectrum (Fig. 2), $K_3V_5O_{14}$ pigment have a strong broad optical absorption from 250 to 560 nm, which is attributed to the energy transfer from O^{2-} 2p orbital to V^{5+} 3d orbital in the VO_n (n = 4 and 5) polyhedral. It is clear that an optical absorption form 400 to 550 nm is due to the VO_5 polyhedron. The pigment showed a higher reflection at the wavelength from 560 nm, which is good matched to the emission band of the $K_3V_5O_{14}$ pigment. As a result, The $K_3V_5O_{14}$ pigment showed a bright-vivid red body color and the L*, a* and b* values were 52.1, 35.75 and 19.06, respectively.
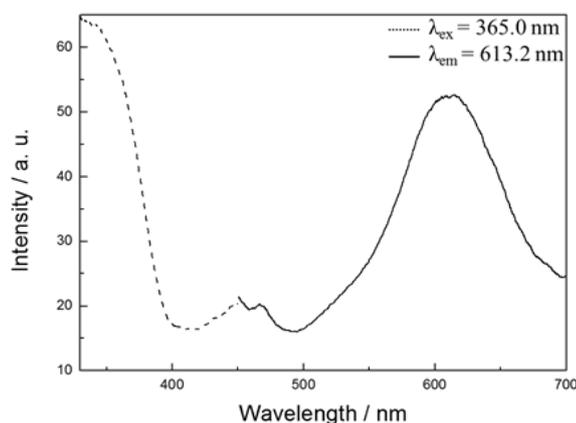
Fig 1. Excitation and emission spectra of $K_3V_5O_{14}$ sample after annealing treatment at 400ºC.
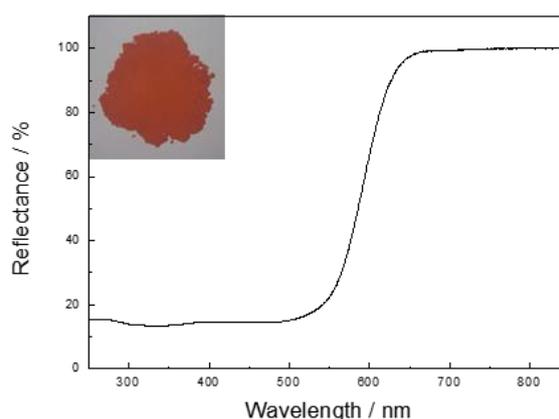
Fig 2. UV-vis diffuse reflectance spectrum of $K_3V_5O_{14}$ pigment after annealing treatment at 400ºC.

Improvement of uniformity in hardness distribution of die-quenched products in hot stamping using rapid resistance heating

Tomoyoshi Maeno[*1], Ken-ichiro Mori, Masato Sakagami[2], Yoshitaka Nakao[2]

[1]Division of Materials Science and Chemical Engineering, Faculty of Engineering, Yokohama National University

[2]Department of Mechanical Engineering, Toyohashi University of Technology

Yokohama, Kanagawa 240-8501, Japan, Toyohashi, Aichi 441-8580, Japan
TEL: +81-45-3393447   E-mail: maeno-tomoyoshi-yf@ynu.ac.jp

Abstract To improve the uniformity in hardness distribution of die-quenched products, the hardening behaviour of a quenchable steel sheet for hot stamping using rapid resistance heating was examined in a hot bending experiment. The sheet was heated to 900 °C in several seconds. The effect of the heat treatment before hot stamping on quenchability in die quenching was examined. The quenchability was improved by normalising heat treatment because the grain size reduced. Standard deviation of the hardness in the sheet heated to 900 °C in 3.2 s without holding at the austenitising temperature was 3%, whereas the deviation reduced to 1% for holding at the austenitising temperature of 3 s.

Experimental To investigate the hardening behaviour in hot stamping using resistance heating, a hot hat-shaped bending process using resistance heating was performed. The equipment for resistance heating and the bending dies were installed in a 1500 kN CNC servo press. A typical quenchable steel sheet 22MnB5 without coating was used for the experiment. The heating temperature was 900 °C. The heating rate v and holding time at austenitising temperature t were changed. The blank was heated by passage of direct current for several seconds. The heated blank was released from the holder immediately after heating, and was transferred to the hat-shaped bending dies. Furthermore, the effect of grain size of the steel sheet before hot stamping on the die-quenchability was examined with the normalised and annealed sheets.

Results and Discussion In Fig. 1, as the grain size increases, the hardness decreases. For the large grains, the heating time is too short to diffuse carbon in the cementite phase sufficiently. Hardening of the hot-stamped pars becomes insufficient because of the insufficient austenitisation. The effect of holding time at austenitising temperature on the hardness of die-quenched parts is shown in Fig. 2. As the holding time at the austenitising temperature increases, the hardness slightly increases up to t = 5 s. The standard deviation of the hardness is remarkably reduced by holding at the austenitising temperature above 1 s.
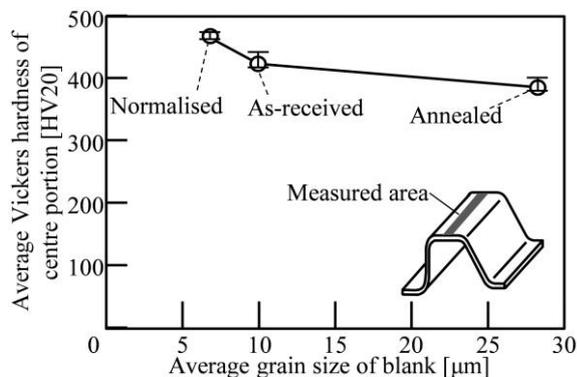
Fig.1 Effect of grain size of steel sheet before hot stamping on Vickers hardness after die quenching in hot stamping using resistance heating for v = 275 °C/s and t = 0 s.
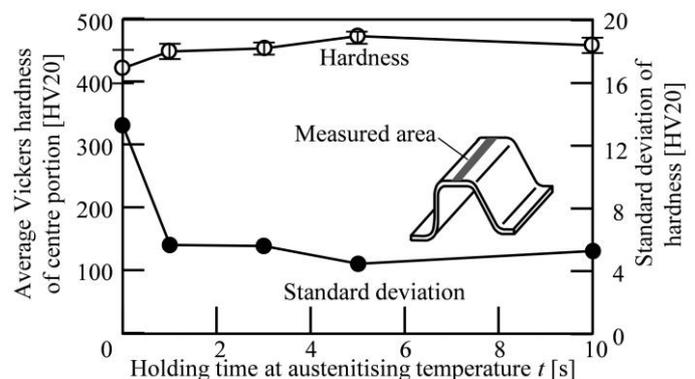
Fig.2 Effect of holding at austenitising temperature on Vickers hardness and standard deviation for v = 275 °C/s.

Effect of Heat Treatment on Microstructure Evolution and the Tensile Properties of Haynes 282 Superalloy

Kyeong-Yong Shin[1], Byeong-Ook Kong[2], Sung-Tae Kang[2] and Hyun-Uk Hong[1]*

Changwon National University[1], Doosan Heavy Industries & Construction[2]

[1] *20 Chanwondaehak-ro,Changwon, Gyeongnam 51140, Republic of Korea*
[2] *22 Doosan volvo-ro, Changwon, Gyeongnam 51711, Republic of Korea*
*TEL: +82-55-213-3699   E-mail: *huhong@changwon.ac.kr*

Abstract In the present study, the effects of three different cooling rates and different aging treatments were studied to identify their influences on γ' formation and microstructure evolution in Haynes 282. The high temperature properties, deformation behavior and fracture characteristics were investigated at 750˚C. The results showed the yield strength of 1step aging following water cooling was higher than 2step aging heat treatment. An attempt has therefore been made to correlate the tensile properties and dislocations' characteristics with the observed deformation mechanisms under different heat treatment conditions. As a result, the dislocation behavior is changed from stacking fault shearing mechanism to Orowan bypass mechanism while coarsening the γ'.

Experimental The Haynes282 alloy has chemical composition of 20Cr-10Co-8.5Mo-2.1Ti-1.5Al-1.5Fe-0.3Mn-0.2Si-0.06C-0.005B and Ni as the balance. The samples of this alloy were conducted into different three cooling rate after solution treated at 1135˚C for 20min. Also, Different aging heat treatment was carried out as not only one step aging heat treatment, which is heated at 800˚C for 4hr, but also two step aging heat treatment, which is heated at 1010˚C for 1hr following 788˚C for 8hr. The tensile test was proceeded at 750˚C. The samples for initial and deformed microstructure observation were analyzed by scanning electron microscope (SEM) and transmission electron microscope (TEM).

Results and Discussion The tensile test is conducted at 750˚C. As a result, Only, The yield strength of 1step aging heat treatment following water cooling is higher than 2step aging heat treatment. The dislocation is different deformation mechanism not only shearing but also bypassing. In 1step aging heat treatment after water cooling, the dislocation is appeared as stacking fault shearing by cutting the γ'. On the other hands, others is formed as Orowan looping by bypassing the γ'.
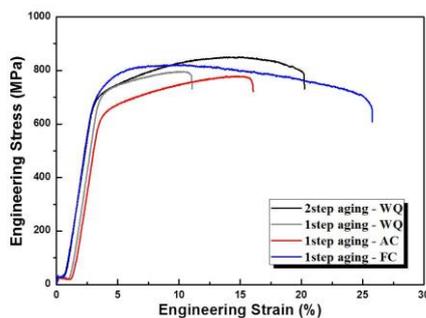
Fig.1 Tensile curves of Haynes 282 at 750ºC for the various heat treatment
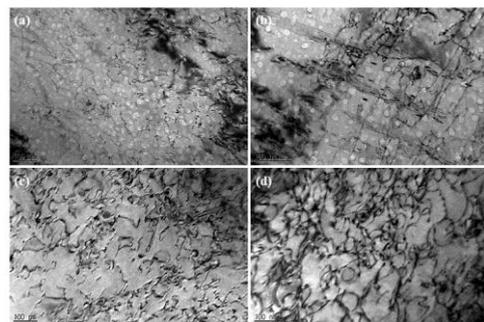
Fig.2 TEM Bright field images showing the dislocation behavior after tensile test at 750ºC : (a) 2step aging   heat treatment following water cooling, 1step aging   heat treatment following (b) water cooling, (c) air cooling and (d) furnace cooling.

References
1) Y. Yuan et al., Scripta Materialia 67, 137-140, 2012
2) F. Sun et al., Journal of Alloys and Compunds 687, 389-401, 2016
3) J.N. Wagner et al., Materials Science & Engineering A 662, 303-307, 2016

A Review of subsurface crack initiation models in high-cycle fatigue for titanium alloys

Weibo Li [1], Osamu Umezawa[2]

1. Graduate School of Engineering, Yokohama National University, 79-5 Tokiwadai, Hodogaya, Yokohama, 240-8501, Japan

2. Faculty of Engineering, Yokohama National University79-5 Tokiwadai, Hodogaya, Yokohama, 240-8501, Japan

TEL: +81-45-339-3873   E-mail: li-weibo-wv@ynu.jp

Fatigue crack initiation is generally understood to occur on a specimen surface due to irreversible process of extrusion and intrusion through slip deformation. The subsurface fatigue crack generation in titanium alloys, however, has been commonly reported in high-cycle regime and at low temperature.[1-3] The alloy composition, microstructure and loading condition markedly affect crack generation, and the initiation sites are not associated with pre-existing defects. The subsurface crack initiation sites appear crystallographic facet or facets in both near α and α-β types titanium alloys. Based on the linear mechanics evaluation for the subsurface crack propagation, the crack initiation stage may consume major part of fatigue life.[2,4,5] However, subsurface fatigue crack initiation does not exhibit direct evidence of cracking and macroscopic support. A number of studies have been done to clarify the subsurface fatigue crack generation for titanium alloys and some models have been proposed how the facet may be formed. Dislocation movement of titanium alloys was fairly planar and dislocation arrays were piled up in the vicinity of grain boundaries.[2,6] Then the local stress concentration near the grain boundary due to the heterogeneous slip may cause the subsurface fatigue crack generation and lower the high-cycle fatigue strength. To relax the concentrated stress, a deformation or microcracking may generate in the adjacent grain. However, no evidences have shown the microcrack initiated at the localized deformation structure directly. The characterization of subsurface fatigue crack initiate sites of near α and α-β types titanium alloys and their cracking models proposed were reviewed to make unknown issues clarified in the previous works.

The subsurface crack initiation of near α and α-β types titanium alloys is common in both dwell fatigue and high-cycle fatigue. The facets formed under different loading conditions seem qualitatively similar, and most of the facets form on or near the basal plane. The heterogeneous micro-plasticity deformation due to planar slip and restricted system remarkably cause subsurface fatigue crack, on which stress redistribution may play an important role. However, it has not been clear what kinds of stresses on the basal plane provide the facet formation such as tensile stress, shear stress and their combination.

The crack initiation sites consisted of facets mostly on near basal plane of α grain, although the crystallographic orientation and surface topography of the facets presented a subtle difference. The crack initiation mechanisms were a quasi-cleavage accompanying high normal stress on the plane, a combination of basal slip and normal stress across the basal plane, and a pure slip on facet plane inclined near 45 degree to loading axis.

References
[1] O. Umezawa, et al., Advances in Cryo. Eng. Mater., Vol.60 AIP Conf. Proc. 1574 (2014) 34-41.
[2] O. Umezawa and K. Nagai, ISIJ Inter., 37 (1997) 1170-1179.
[3] O. Umezawa, et al., Advances in Cryo. Eng. Mater., Vol.40 (1994) 1231-1238.
[4] M. Hamada and O. Umezawa, ISIJ Inter., 49 (2009) 124-131.
[5] O. Umezawa, M. Hamada and T. Tatsumi, Procedia Materials Science, 12 (2016) 48-53.
[6] H. Yokoyama, et al., Metall. Mater. Trans. A, 31A (2000) 2793-2805.

Fabrication and Characterization of Ag-SiO₂ / Inorganic Antimicrobial coating agent

Hyeon-Tae Im, Dong-Sik Bae†

Department of Advanced Materials Engineering, Changwon National University

20 Changwondaehak-ro Uichang-gu Changwon-si, Gyeongsangnam-do 641-773 KOREA
TEL: +81-55-275-5475 E-mail: dsbae7@changwon.ac.kr

Abstract In recent years, attention has been increasingly focused on the problem of the environment by all over the world and the desire to enjoy a pleasant life has been reflected in the concept of 'environmentally friendly' living environment. This study is concerned with the development of antimicrobial coatings for preventing contamination and increasing antimicrobial activity. Antimicrobial coating agents are compounds that inhibit or kill microorganisms. Antimicrobial coatings are applied to the surface of daily necessities, medical devices, industrial products, electrical appliances, fabrics, and interior building materials, etc.

Experimental In this experiment, the Ag-SiO2 particles was prepared by sol-gel method. The inorganic hybrid binder was manufactured by sol-gel method. It was prepared by a silica compound such as silica-sol and TEOS. Synthesized coating sample was manufactured using coating solution that was proceeded by ball-milling method for 6hr by the addition of Ag-SiO2 nanoparticles. The microstructure and composition of the coating layer measured by SEM and EDS. The physical properties were characterized by pencil hardness, level of adhesion and salt spray. Disk diffusion test was easy and objective testing method on the antibacterial activity of antibacterial agent itself.

Results and Discussion In this study, the Ag-SiO2 / inorganic antimicrobial coating agent was formed to 10μm ~ 25μm coating thickness and microstructure that judged the Ag-SiO2 particles were uniformly well distributed on coating layer. The results of adhesive and hardness measurements were investigated having adhesive property was excellent as 5B. The hardness was as 8H. The higher the Ag-SiO2 particles, the better the stain resistance and the antimicrobial activity.
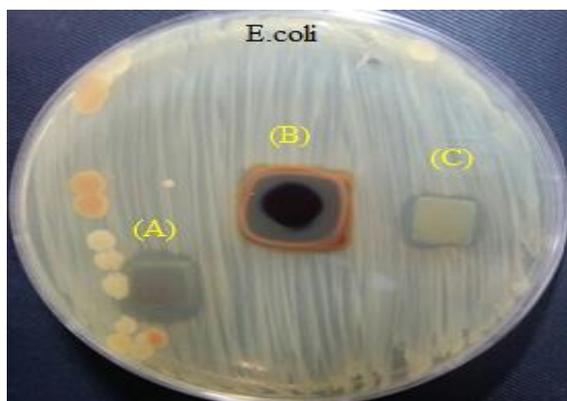
Fig.1 Disk diffusion test of synthesized by Ag-SiO2 nanoparticles and inorganic binder; (A)5g, (B)0g and (C)2g
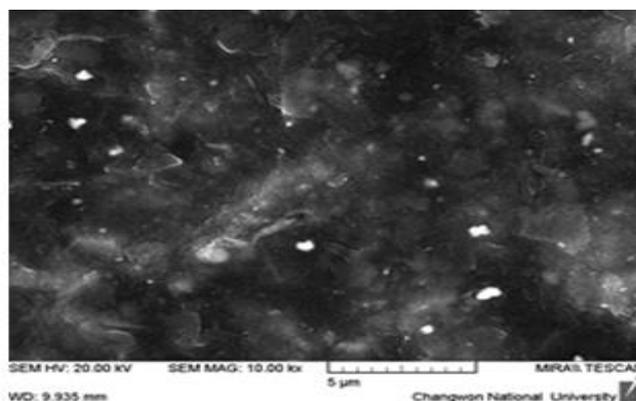
Fig.2 FE-SEM image of synthesized by Ag-SiO2 nanoparticles and inorganic binder.

References

1) Kugel AJ et al., Combinatorial materials research applied to the development of new surface coatings XII: novel, environmentally friendly antimicrobial coatings derived from biocide-functional acrylic polyols and isocyanates. J. Coat. Technol. Res., 6, 107 (2009)

2) Limei Chen et al., Chemical assembly of silver nanoparticles on stainless steel for antimicrobial applications, Surface & Coatings Technology, 204, 3871 (2010)

3) Klasimir Vasilev et al., Antibacterial Surfaces for biomedical devices, Expert Rvi. Med. Devices., 6, 553 (2009)

The prospect of Metal Additive Manufacturing towards performance and innovations

Mathieu Terner[1,2], Sara Biamino[2], Jeong-Seok Lee[1]

[1]Changwon National University, [2]Politecnico di Torino

[1]20 Changwondaehak-ro, 51140 Changwon-si, Republic of Korea,
[2]Corso Duca degli Abruzzi 24, 10129 Turin, Italy

TEL: +82-55-213-3698   E-mail: mathieu@changwon.ac.kr

Abstract: Powder-based Metal Additive Manufacturing has emerged for a few years as an encouraging solution for the production of metal parts with outstanding characteristics. Additive Manufacturing is acknowledged to offer exceptional advantages including complexity for free, near-net-shape production and waste reduction. A unique set of materials properties is also obtained. The present communication reports encouraging production of Ti-based alloys by means three different Additive Manufacturing processes. First, the production of γ-TiAl alloys by Electron Beam Melting (EBM) for application in gas turbine engines is described in details. The materials exhibited excellent specific properties analogous to heavy-weight superalloys. Second, the production of the well-known Ti-6Al-4V alloy by Selective Laser Melting (SLM) is reported. The importance of optimizing the energy density during the process is in particular highlighted. At last, an innovative production of Ti-6Al-4V by means of Digital Light Processing (DLP) is described. Initially limited to the production of plastics parts, properly mixing powders with the liquid photopolymer allows producing a composite which may be ultimately sintered into a porous metallic part.

Experimental: 3rd-generation γ-TiAl based powders were used as starting materials for the EBM process, in which the parts are built layer-by-layer by selective fusion of the powder under vacuum pressure by a high energy electron beam. The numerous process parameters were optimized to reduce residual porosity. Subsequent heat treatments in vacuum were studied to tailor the microstructure towards optimum mechanical properties for gas turbine engine structural applications. For the SLM production of Ti-6Al-4V, fine pre-alloyed powders were used as starting materials. The selective fusion of the powder is realized in controlled atmosphere with a laser beam as the energy source. The process parameters were controlled and their effect were studied, namely the laser power, hatch spacing, scanning speed, layer thickness and scanning strategy. The microstructure and porosity were observed. Finally, recycled unprocessed Ti-6Al-4V powders from the previous SLM processing were used for DLP to maintain the costs as low as possible. Here, the process is a photopolymerization process, which involves selective solidification of liquid curable resins by ultraviolet radiation. A high content of powder was mixed with an acrylate-based photo-curable resin with addition of appropriate additives (i.e. surfactants). The resulting slurry was then processed using a custom DLP apparatus.

Results and Discussion: The γ-TiAl alloys produced by the optimized EBM trial exhibited high homogeneity, very low impurities pick-up, very low residual porosity << 1 % and a fine near-γ microstructure (Fig.1A). Any of the typical microstructures of γ-TiAl alloys could be set-up by careful heat treatment under vacuum in the vicinity of the α-transus temperature. The nearly lamellar microstructure (Fig.1B), consisting in

roughly 80 % of lamellar colonies with an average size of about 140 μm pinned at their boundaries by equiaxed γ-grains smaller than 50 μm, showed in particular excellent oxidation resistance and encouraging specific strength and creep resistance similar to that of equivalent Ni-based superalloys used for high temperature structural applications. At roughly half the density of that of Ni-based superalloys, this makes γ-TiAl alloys great candidates for rotating high-temperature structural components in gas turbine engines. The Ti-6Al-4V alloys produced by SLM exhibited mechanical properties significantly lower than conventional Ti-6Al-4V. Observation of the microstructure confirmed that the very quick solidification caused by the process lead to the formation of the martensitic α' microstructure, in place of the desirable α+β. In addition, the level of residual porosity was rather high. This suggests that the SLM process may be optimized by varying the energy density value, as well as the microstructure by proper heat treatment. Finally, an appropriate composition for a metal-powder rich photo-curable slurry was found with addition of a dispersant and an anti-settling agent in solution. Despite clear difficulties to cure the slurry caused partly by the low concentration of photosensitive compound, a composite layer was successfully produced (Fig.2). However, much work has to be conducted to optimize the composition of the slurry in order to allow fast curing and multi-layer processing. This challenging innovative manufacturing method yet offers encouraging considerations.
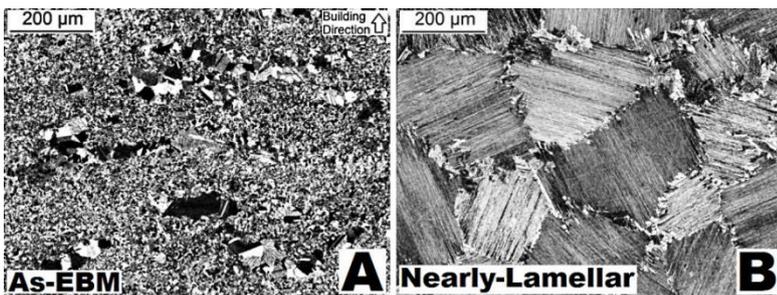
Fig.1: Microstructure of Ti-45Al-2Cr-8Nb A: as-EBM and B: Nearly-Lamellar after heat treatment

Fig.2: One-layer Ti64-photopolymer composite produced by Digital Light processing

The stability of retained austenite and transformation behaviour in TRIP steels at low temperature

Takayuki Yamashita[1], Norimitsu Koga[2], Osamu Umezawa[2]

1. Graduate School of Engineering, Yokohama National University, 79-5 Tokiwadai, Hodogaya, Yokohama, 240-8501, Japan

2. Faculty of Engineering, Yokohama National University79-5 Tokiwadai, Hodogaya, Yokohama, 240-8501, Japan

TEL: +81-45-339-3873   E-mail: yamashita-takayuki-yz@ynu.jp

Introduction

Low alloy multiphase steels associated with transformation-induced plasticity (TRIP) of retained austenite (γ_R) shows a good balance of tensile strength and ductility, since the TRIP causes to maintain higher work-hardening rate in the high strain regime.[1] Then the stability of γ_R is a key factor to control the TRIP effect.[2],[3] Although the stability of γ_R depends on various factors such as chemical compositions, morphology and size of austenite, the transformation behaviour of individual γ_R has not been clear. In the present study, the influence of stability of γ_R on work-hardening and transformation behavior at low temperature has been investigated for TRIP steels with different chemical compositions.

Experimental

Two types of low alloy TRIP steel sheets with different volume fraction of γ_R (low-γ: 9.4% and High-γ: 17.2%) containing about 1.3 mass% C were used. The steels were cold-rolled and annealed at 1063 K in $\alpha+\gamma$ region, and then cooled to 673 K for austempering. Tensile tests were carried out at 77 K, 193 K, 233 K and 293 K. The microstructure and crystal orientation of TRIP steels were analyzed using electron backscattered diffraction (EBSD). The microstructure consists of ferrite matrix (α_f), bainite (α_b) and γ_R. The γ_R grains were distributed in α_f grains and at the grain boundaries between α_f and α_b.

Results and Discussion

The steels showed high ductility and tensile strength at 193 K, 233 K and 293 K. The tensile strength of steels at 77 K was much higher than that of other test temperatures, although the steels exhibited early fracture. The work-hardening rate was increased with decreasing test temperature. At 193 K and 233 K, the rate was kept with high value in the high strain regime. The stability of γ_R at 293 K was much higher than that of other test temperatures. The γ_R at 233 K and 193 K at 10% strain was mostly transformed. Then the difference of the work-hardening rates among the temperatures may depend on the stability of γ_R and the strengthening of α_f at lower temperature, although the influence of TRIP on ductility has not been clear yet.

The most of γ_R grains after tensile test at 193 K, 233 K and 293 K revealed the orientation near <111> parallel to the tensile direction, in which their Schmid factors were low as shown in Table 1. It suggested that the deformability of γ_R commonly affected to the martensitic (α') transformation in the steels at 293 K. The volume fraction of γ_R at 77 K was less than 1% at 3% strain, the most of γ_R were transformed to α' under stress concentration. The work hardening rate at 193 K, 233 K and 77 K in the steels may depend on their volume fraction of γ_R.

References
[1] M. TAKAHASHI: *Nippon Steel Technical Report,* 88 (2003), 2
[2] K. SUGIMOTO, M. KOBAYASHI, S. HASHIMOTO: *Metall. Trans.*, 23A (1992), 3085
[3] A. ITAMI, M. TAKAHASHI, K. USHIODA: *ISIJ int.*, 35 (1995), 1121
[4] T. YAMASHITA, N. KOGA, O. UMEZAWA: *CAMP-ISIJ*, 29 (2016), 346

Atom probe study of the precipitation of κ-carbide with Si addition and dislocation behavior in a cast FeMnAlC lightweight steel

Chi Won Kim[1], Jae Hyun Lee[1], Jun Oh Moon[2], Jae Hoon Jang[2], Seong Joon Park[2], Bong Ho Lee[3], Young Joo Lee[4] and Hyun Uk Hong[1*]

[1]Department of Materials Science and Engineering, Changwon National University, [2]Ferrous Alloy Department, Korea Institute of Materials Science, [3]Daegu Gyeongbuk Institute of Science and Technology, [4]Research Institue of Industrial Science and Technology

[1]20 Changwondaehak-ro, Uichang-gu, Changwon, Gyeongnam 51140, Republic of Korea
[2]797 Changwondaero, Sungsan-gu, Changwon, Gyeongnam 51508, Republic of Korea
[3]333 Techno-jungangdaero, Dalseong-gun, Daegu 42988, Republic of Korea
[4]67 Cheongamro, Nam-gu, Pohang, Gyeongbuk 37673, Rpublic of Korea

TEL: +82-55-213-3699   E-mail: *huhong@changwon.ac.kr

Abstract

In this work, the investigation of precipitation and deformation behavior has been conducted on the effect of Si addition in a Fe-30Mn-9Al-0.9C cast steel. The result of atomistic analysis reveals partitioning of alloy elements in Si free and 1% Si added steels(Fig.1). Si atoms are partitioned in the interface of κ-carbide/γ-matrix and C atoms are excessively partitioned in κ-carbide in a 1% Si steel (Fig.1b). Si addition affects dislocation behavior to cut through κ-carbides resulting in Shearband-Induced-Plasticity (SIP) (Fig.2).

Experimental

Hardness was measured for aged Si free and 1% Si steels at 550°C for 100 hours. 3D-APT revealed compositional distribution on the Si addition. Deformation microstructures were observed by means of TEM. Also, calculation of the first principle was conducted to elucidate the effect of Si addition on the evolution of deformation microstructure.

Results and Discussion

Si addition contribute to not only the C-partitioning into κ-carbides but also change of deformation microstructure. C-enriched κ-carbide in the 1% Si steel effectively retards dislocation movement due to increased coherency strain and formation of unfavorable Al-C bonding by shearing κ-carbides. In the first principle calculation, more C atoms are partitioned in κ-carbide more energies are required to shear κ-carbides.
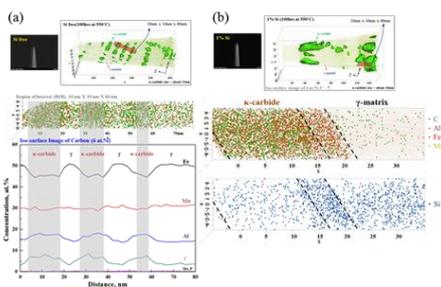
Fig.1 Compositional distribution observation of Si free and 1% Si added steel by 3D-APT.
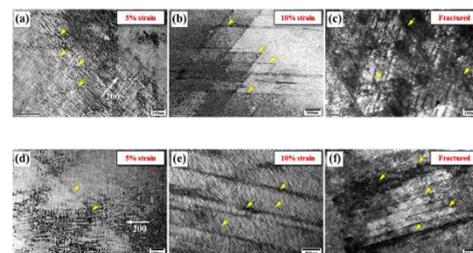
Fig.2 Evolution of deformation microstructure of Si free and 1% Si added steel by TEM.

References

1) C.W. Kim, S.I. Kwon, B.H. Lee, J.O. Moon, S.J. Park, J.H. Lee, H.U. Hong, Atomistic study of nano-sized κ-carbide formation and its interaction with dislocations in a cast Si added FeMnAlC lightweight steel, Mater. Sci. Eng. A 673 (2016) 108-113

Thermodynamic Assessment and Determination of Phase Diagram Including Spinodal Lines in Al-Mg Alloy

Shosuke Kogo[1*], Hideaki Iwaoka[1], Shoichi Hirosawa[1]

[1]Depart. Mechanical Engineering and Materials Science, Yokohama National University;

79-5 Tokiwadai, Hodogaya-ku, Yokohama-shi 240-8501, JAPAN
Corresponding author. TEL: +81-45-339-3857   E-mail: kogo-shosuke-dg@ynu.jp

Abstract Although several thermodynamic modelling have been carried out for the Al-Mg alloy system, no previous thermodynamic descriptions could calculate the metastable phase diagram of $L1_2$-type ordered GP zones (Al_3Mg). In this study, Calphad-type thermodynamic assessment (Fig. 1) of Al-Mg binary alloys was performed to determine not only the miscibility gap but also the spinodal lines of GP zones. The Gibbs energies of fcc-Al solid solution and ordered GP zones were expressed by a four-sublattice model (split compound energy formalism), and a complete thermodynamic description was obtained from available experimental data. The miscibility gap and spinodal lines calculated from the optimized parameters could satisfactorily reproduce available experimental data for the equilibrium between fcc solid solution and ordered GP zones (Fig. 2).

Calculation Method GP zone is a coherent precipitate with $L1_2$-type ordered structure, and the Gibbs energies of both of fcc solid solution and ordered GP zones are needed to calculate the metastable phase diagram. In this study, a thermodynamic model to describe the Gibbs energy of fcc phase was utilized based on a four-sublattice model (split compound energy formalism). All the model parameters were finally determined when achieved a best fit to experimental data; e.g. miscibility gap of GP zones and equilibrium phases, and thermal quantities of mixing enthalpy and activity. All calculations were performed using Pandat and Thermo-Calc software packages.

Results and Discussion The Gibbs energy curve of fcc phase calculated in this study provides a miscibility gap type curve. Therefore, a whole metastable phase diagram of GP zones can be calculated by the estimated thermodynamic description. The calculated miscibility gap and spinodal lines could satisfactorily reproduce experimentally reported reliable data, and thus the equilibrium between fcc-Al solid solution and ordered GP zones was successfully evaluated for the first time.
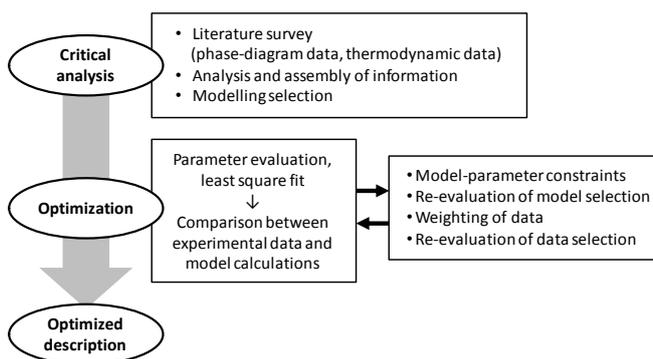
Fig.1 Procedure of thermodynamic assessment utilized in this study.
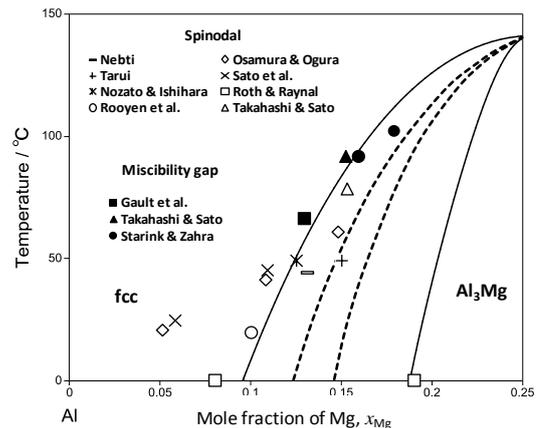
Fig.2 Calculated miscibility gap (solid lines) and spinodal lines (broken lines) of GP zones (Al_3Mg). Experimentally reported data is also shown by symbols.

Analysis of Strain distribution in deformed materials by digital image correlation

Norimitsu Koga[1], Pham Thi Thanh Huyen[2], Osamu Umezawa[1]

1. Faculty of Engineering, Yokohama National University, 79-5 Tokiwadai, Hodogaya, Yokohama, 240-8501, Japan

2. Graduate school of Engineering, Yokohama National University79-5 Tokiwadai, Hodogaya, Yokohama, 240-8501, Japan

TEL: +81-45-339-3873   E-mail:koga-norimitsu @ynu.ac.jp

Introduction

Digital image correlation (DIC) method [1] is adapted to calculating strain from the difference of images between before and after deformation. It is applicable to any materials and deformation modes as long as significant contrasts. We reviewed the principle of DIC method and demonstrated the strain distribution in tensile deformed ferritic steel.

Experimental

Ultra-low carbon steel (Fe-0.008wt%C) was used for demonstrating strain distribution formed by tensile deformation. The material was cold rolled with 80 % in reduction and annealed at 983 K for 1.8 ks followed by water quenching. The average grain size was 25 μm. Tensile test was carried out at 293 K and 77 K. Microstructure was observed by scanning electron microscopy (SEM). SEM images before and after deformation at the same region in etched specimen were taken for DIC analysis. DIC analysis was carried out with VIC-2D software (Correlated Solutions Ltd).

Results and Discussion

Figure 1 shows strain distribution along tensile direction in tensile deformed specimen at 293 K (a) and 77 K (b). Strain is indicated by color bar, maximum and minimum strain are twice average strain and -1 %, respectively. Strain is homogeneously distributed at 293 K (a) while strain distribution at 77 K (b) is markedly inhomogeneous; high strain region is larger than twice average strain and compressive strain is partly observed even though applying only tensile deformation. The high and low strain regions tend to be continuously distributed along 45 degree from tensile direction which is maximum shear stress direction. This inhomogeneous strain distribution at 77 K is caused by restricting the slip system with lowering temperature.
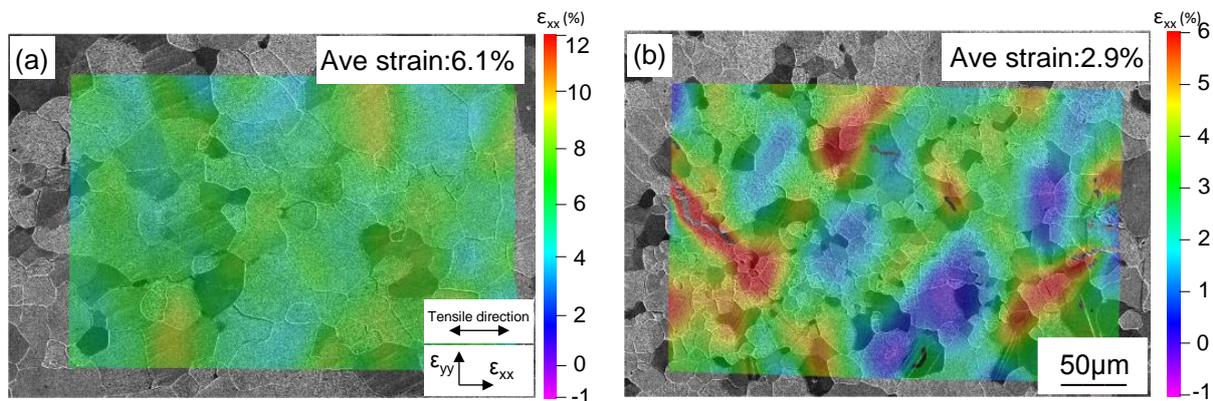
Fig.1 Strain distribution along tensile direction in tensile deformed specimen at 293 K (a) and 77 K (b).

References

1) W. H. Peters, Z.-H. He, M. A. Sutton, W. F. Ranson; Experimental Mechanics, 24 (1984) 117-121.

Morphology of Aluminium (Al 3003) Chemical Etching for Insert Molding

Dong-Gyu Lee, Jeong-Hun Son and Dong-Sik Bae[†]

Department of Advanced Materials Science and Engineering, Changwon National University

Department of Advanced Materials Science and Engineering, Changwon National University,
Changwon, 641-773, Korea
TEL: +82-55-275-5475   E-mail: dsbae7@changwon.ac.kr

Abstract Aluminium has a low reduction potential, and the structure of aluminium surface changes through a chemical etching. The surface area of aluminium increased with chemical reaction. The morphology of etched aluminium surface change according to a kind of etching solution. HCl, $FeCl_3$ and mixed acid used for etching agent in order to increase aluminium surface area.

Experimental The precleaning removed oxide film of Al 3003 at using PURICLE C-4. Thereafter, washing with DI water. The etching solution is etched. The etching solution type was HCl(16.5, 25, 33%), $FeCl_3$(33, 50, 100%) and HCl+$FeCl_3$(20, 33%). Experimental value changed such as reaction temperature and time. Physical washing was performed using ultrasonic. Chemical washing was performed using diluted nitric acid.

Results and Discussion The structure of etched Al 3003 was observed using FE-SEM(field emission scanning electron microscope), OM(optical microscope). As a result of observation, it was confirmed that etch pits were formed from the etched aluminium surface. The change of etch pit with time and temperature was confirmed. Etch pits were formed on the aluminium surface to increase the surface area. The change of the bond strength value with the polymer according to the surface change was confirmed. The surface roughness was checked using a surface roughness tester. As a result of confirm the bonding strength with the polymer using a tensile strength machine, a bonding strength of aluminium and polymer was above 10MPa.
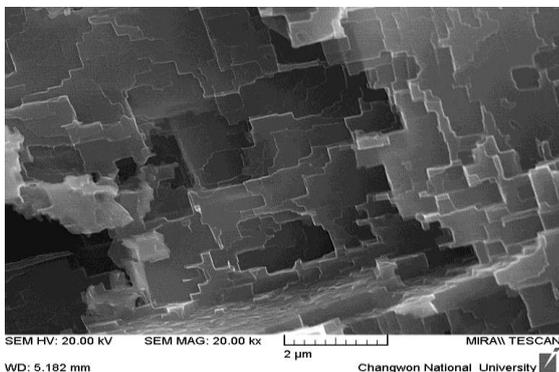
Fig.1 FE-SEM image of Al 3003 with HCl(25%) at 30℃ for 7min
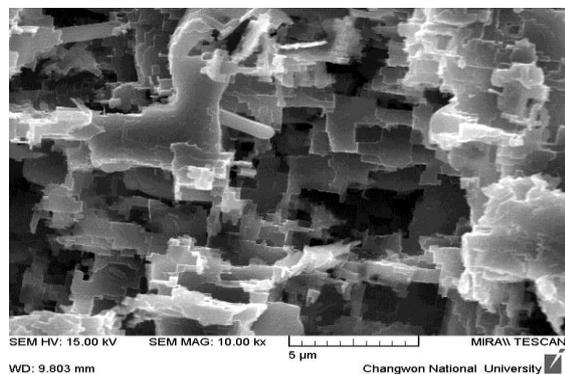
Fig.2 FE-SEM image of Al 3003 with HCl+$FeCl_3$(33%) solution at 30℃ for 7min

References

1) O. Ça kır, "Chemical etching of aluminium"**,** J. Mater. Process. Technol. 199 (2008) 337
2) B. Qian and Z. Shen, "Fabrication of Superhydrophobic Surfaces by Dislocation-Selective Chemical Etching on Aluminum, Copper, and Zinc Substrates", Langmuir 21 (2005) 9007
3) V. Martigovitg, M. Zahoran, I. Kogin~ir and J. Trnovec, "Effect of chemical reaction stoichiometry on the pressure variations in the etching chamber during etching of aluminium", Physics Letters A 173 (1993) 462

Microstructural Change of Thermal Barrier Coatings Deposited on TiAl Alloy

Kotatsu Hirata[*1] and Makoto Hasegawa[2]

[1]Department of Systems Integration, Specialization in Solid State Materials and Engineering, Graduate School of Engineering, Yokohama National University, Japan

[2]Division of Materials Science and Chemical Engineering, Faculty of Engineering,

Yokohama National University, Japan

79-5, Tokiwadai, Hodogaya-ku, Yokohama, 240-8501, Japan
TEL: +81-45-339-3838,   E-mail: hirata-kotatsu-yr@ynu.jp

Abstract Thermal barrier coatings (TBCs) have been widely used to protect the gas turbine blades and vanes from the corrosion, oxidation and high temperature environment. TBCs are composed of thermal barrier coating (TBC) layer and bond coat (BC) layer; TBC layer and BC layer are formed by heat-resistant ceramics and oxidation-resistant alloy, respectively. This system is usually applied to the Ni base superalloy. Recently, in order to improve the low oxidation and creep resistance of TiAl alloy over 1073 K, TBCs are applied to the TiAl alloy substrate. However, change of microstructure in this systems is still not known. In this study, TBCs deposited on TiAl alloy are heat exposed in different temperature and time to observe the microstructural change of the systems.

Experimental Ti-46Al-7Nb-0.7Cr-0.2Ni-0.1Si (mol%) alloy are used for a substrate of TBCs. Co-32Ni-21Cr-8Al-0.5Y (mol%) alloy is deposited on the substrate as BC layer up to 100 μm in thickness by cold spray (CS) process. 4 mol% yittria stabilized zirconia (YSZ) is deposited by air plasma spray (APS) process up to 250 μm in thickness on BC layer as TBC layer. TBCs specimens are heat exposed in an air at 1073, 1173 and 1273 K for 10, 50, 100 and 200 hours. The microstructures of the as-deposited and heat exposed TBCs are observed by scanning electron microscopy (SEM). Change of chemical composition in each layers are measured by energy dispersive X-ray analysis (EDX) and electron probe micro analyzer (EPMA).

Results and Discussion Fig.1 shows the typical example of a polished transverse section of an as-deposited TBCs. TBC, BC and substrate are visible. After heat exposure at 1273 K for 100 h, thermally grown oxide (TGO) layer forms between TBC and BC layer (Fig.2). Analysis of chemical composition indicates that the TGO layer is mainly composed of Al_2O_3. The thickness of TGO layer is increasing with the increase in heat exposure temperature and time. Al depleted zone forms at the vicinity of TGO layer in BC layer due to the formation of Al_2O_3 at TBC/BC interface. Further, new layer has formed at the BC side and TiAl substrate side from the BC/substrate interface. It seems that interdiffusion is occurring during heat exposure at the interface. Ti and Nb are detected in CoNiCrAlY BC alloy and Co, Ni and Cr are observed in TiAl substrate.
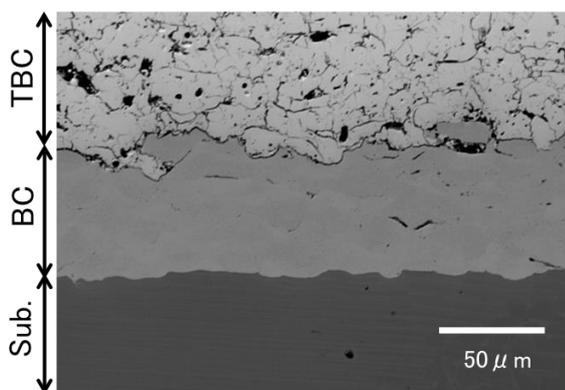
Fig.1 Scanning electron micrograph of as-deposited TBCs.
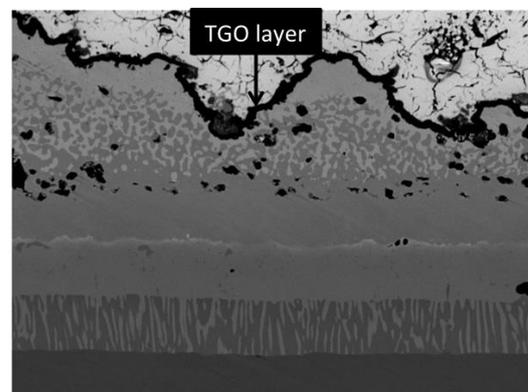
Fig.2 Scanning electron micrograph of the TBCs heat exposed at 1273 K for 100 h.

Synthesis and Characterization of $K_2Ti_6O_{13}$ Whisker by Flux Method

Yeon Bin Choi[1], Jeong Hun Son[1] and Dong Sik Bae[1†]

Department of Advanced Materials Science and Engineering, Chnagwon National University[1]

Department of Advanced Materials Science and Engineering, Changwon National University,

Changwon, Gyeongnam, 641-773, South Korea[1]

TEL: +82-55-275-5475   E-mail: dsbae7@chanwon.ac.kr

Abstract Potassium titanate whisker using for brake lining material in automotive brake systems. $K_2Ti_6O_{13}$ whisker are a major role in preventing light-hazardous materials to asbestos dust generated during automobile braking and improves the wear resistance more than twice the asbestos brake lining. $K_2Ti_6O_{13}$ whisker have been synthesized by a flux method. The average size and distribution of the synthesized $K_2Ti_6O_{13}$ whisker can be controlled by mole ratio of potassium precursor, reaction temperature and time. The average size of the synthesized $K_2Ti_6O_{13}$ whisker was about in the size range of 500nm to 1um and diameter range of 20 to 50nm. The size distribution of the synthesized $K_2Ti_6O_{13}$ whisker was uniform. The synthesized $K_2Ti_6O_{13}$ whisker was characterized by X-ray diffraction (XRD), Field Emission Scanning Electron Microscope (FE-SEM), Energy Dispersive X-ray Spectroscopy (EDS).

Experimental KOH, KNO_3, K_2CO_3 concentration of condition 4, 5 was added to TiO_2 and KCl was added to improve morphology of whisker as a flux. The mixed powders were homogeneously mixed by ball-milling or mixer. The mixed powder was placed in a box furnace, sintering at 850 ~1150℃ for 0.5~4 hours and then quenching at 950°C. After quenching, powder was washed for five times using distilled water (D.I. Water) to remove KCl. Thereafter, it was dried at 100°C for 24 hours.

Results and Discussion The aspect ratio of the synthesized $K_2Ti_6O_{13}$ whisker was decreased with adding potassium chloride as flux and quenching reactant. The measured aspect ratio of the synthesized $K_2Ti_6O_{13}$ whisker was less than 10 when reacted at condition 5. The average length of the synthesized $K_2Ti_6O_{13}$ whisker was about in the range of 1um to 10um. The average diameter of the synthesized $K_2Ti_6O_{13}$ whisker was about in the range of 500nm to 1um.
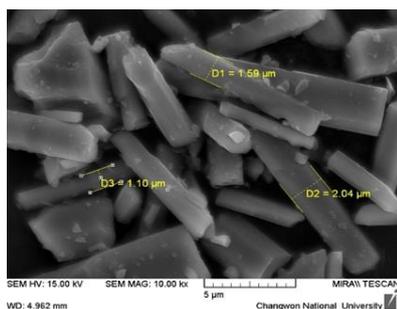
Fig. 1. FE-SEM image of potassium titanate whisker synthesized by Flux method at condition 5 with flux X & quenching O
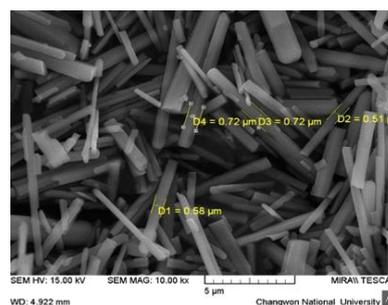
Fig. 2. FE-SEM image of potassium titanate whisker synthesized by Flux method at condition 5 with flux O & quenching O

References

[1] M. A. Siddiquia, V. S. Chandel and A. Azam, ''Comparative study of potassium hexatitanate ($K_2Ti_6O_{13}$) whiskers prepared by sol–gel and solid state reaction routes'', Appl Surf Sci. 258 (2012) 7354.

[2] T. Endo, H. Nagayama, T. Sato and M. Shimada, ''Crystal growth of poatassium titanates in the system K_2O-Fe_2O_3-TiO_2'', J Cryst Growth. 78 (1986) 423.

Lecture 013

Effect of Preparation Methods on the Electrochemical
Performance of All-solid-state Li-S battery

Han Ul Choi, Ju Sung Jin, Hyung-Tae Lim[*]

School of Materials Science and Engineering, Changwon National University

20 Changwondaehak-ro, Changwon, Gyeongnam 641-773 Korea
TEL: +82-55-213-3716   E-mail: htaelim@changwon.ac.kr

Abstract

Lithium/sulfur (Li-S) batteries are one of the most promising rechargeable storage devices due to their high energy density (~ 2, 500 Wh/kg), which is ~ 5 times higher than that of lithium ion batteries[1, 2]. All-solid-state Li-S batteries were fabricated with lithium silicide anodes ($Li_{4.4}Si$), sulfide-based glass electrolyte (Li_2S-P_2S_5), and sulfur composite cathode. The sulfur based composite cathode was prepared by two methods; (Case 1) mortar-mixing and (Case 2) planetary ball milling at a rotation speed of 370 rev/min for 10min. SEM analysis results indicate that 'Case 2' method improved distribution of sulfur, carbon and solid electrolyte particles, with the reduction of particle size. This effect was reflected in impedance spectra, and eventually charge-discharge capacity: the electrode/electrolyte interface resistance was reduced so that the average charge-discharge capacities increased in 'Case 2'. Thus, the present work indicates the preparation method of sulfur composite cathode profoundly affects the performance of solid state Li-S batteries.
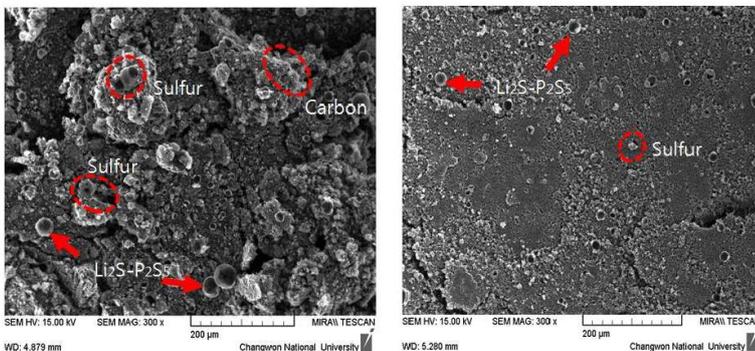
Fig.1 SEM Images of sulfur composite powders prepared by Case 1 (a) and Case 2 (b)
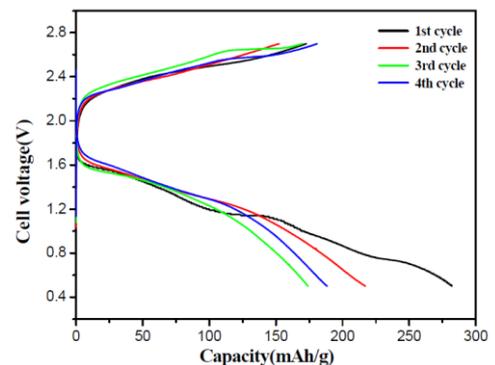
Fig.2 Galvanostatic charge/discharge voltage curves of Case 2

References

1) T. Kobayashi, Y. Imade, D. Shishihara, K. Homma, M. Nagao, R. Watanabe, T. Yokoi, A. Yamada, R. Kanno and T. Tatsumi, *J. Power Sources.* **182,** 621 (2008).
2) M. Nagao, A. Hayashi and M. Tatsumisago, *Electrochim. Acta,* **56,** 6055 (2011).

Control of Electron Coupled State in Superlattice of PbS Quantum Dots by Replacing Ligands

Fumimasa Suetsugu, Keisuke Niwa, Kohki Mukai

Graduate School of Engineering, Yokohama National University

79-5 Tokiwadai, Hodogaya-Ku, Kanagawa, 240-8501, Japan

TEL: +81--45-339-3853 E-mail: mukai-kohki-cv@ynu.ac.jp

Abstract We report that the emission wavelength of superlattice prepared by dense packing of colloidal PbS quantum dots (QDs) became longer by replacing the ligands with shorter ones. The dense packing was achieved by the aid of pyramidal hole array prepared on Si substrate using facet selective etching. Emission energy shift was accompanied with the increase of emission lifetime. These emission properties were attributed to the de-localization of electron wavefunction in the ground state of QD superlattice.

Experimental We investigated chain lengths, replacement methods, and optical properties of ligands to be replaced. Chain lengths of various ligands were compared by using the calculation. After the selection, replacement of ligands was performed. The successful replacement was confirmed by fourier transform infrared (FT-IR) spectroscopy and transmission electron microscopy (TEM) . To compose superlattice film, PbS QDs were deposited in solvent into the pyramidal hole array prepared on Si substrate(Fig.1)[1]. The pyramidal hole array is effective to achieve QD ordering with long periodicity. Scanning electron microscope and atomic force microscope were used to evaluate the arrangement of QDs. Photoluminescence (PL) spectra and emission lifetime were measured by using conventional lock-in system and time correlation measurement system.

Results and Discussion As candidates of ligands to be replaced, n-butylamine (BA), 2-methyl-2-propanol, pyridine (PD), octylamine, oleic acid (OA), trioctylphosphine, oleylamine (OLA) were studied. The calculation by the semi-empirical molecular orbital method and the energy minimization method was done using the free software "Winmostar"[2]. As a result of the studies, we selected BA and PD, which are shorter than OA used in our previous work, and OLA, which are longer than OA, for comparison. We first replaced ligands from OA to BA. We observed the QD interval became shorten by TEM measument, and the peak appearance in FT-IR spectra, that suggests the ligand replacement was successful. Then, we precipitated OA and BA treated QDs on the pyramidal hole arrays for 3 days, respectively. As result of the PL measurement, we observed the emition peak shift for 190nm by forming films of BA-treated QDs, that was not clearly seen using OA-treated QDs. We also confirmed the emition lifetime becoming longer by forming films of BA-treated QDs and observed QDs ordering in the film. These results suggest that the dense packing of BA-treated PbS QDs resulted in the de-localization of electrons at the ground state in QD superlattice, rather than the mere coupling of neighboring ground-state electrons. We will also report details including the results of other ligands.
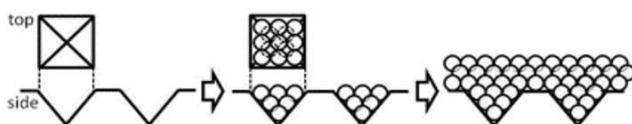
Fig.1 Method to realize long periodic QD structure with pyramidal holes on Si substrate.
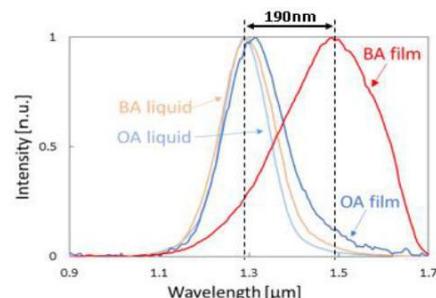
Fig.2 PL spectra of BA-treated and OA-treated PbS QD in liquid and film, respectively.

References

[1] K. Mukai et al., Semicond. Sci. Technol., vol.30, pp.044006 (2015)

[2] X-Ability Co.,Ltd, https://winmostar.com/jp/

The effect of hydrogen sulfide(H2S) on sulfur poisoning of nickel-yttria stabilized zirconia(Ni-YSZ) anode supported solid oxide fuel cells

Hyun Mi Lee, Hyung-Tae Lim[*]

School of Materials Science and Engineering, Changwon National University

20 Changwondaehak-ro, Changwon, Gyeongnam 641-773 korea
TEL: +82-55-213-3716   E-mail: htaelim@changwon.ac.kr

Abstract Solid oxide fuel cells(SOFCs) operate under various type of fuel, such as biogas and syngas, due to their high operating temperature($>700\,℃$) without the need of pre-reforming. H_2S poisoning is an important issue for solid oxide fuel cells operated with biogas and syngas[1-3]. This study investigates the effect of hydrogen sulfide (H_2S) concentration of Ni/YSZ anode-supported degradation rates of SOFCs. The electrochemical impedance spectra (EIS) of the cells were measured in pure hydrogen fuel and compared to H_2S additives (before poisoning). The performance degradation was studied with concentration of H_2S (0~50ppm) at $700\,℃$ under a constant current($500mA/cm^2$) condition. In all cases, the H_2S contained in the fuel caused a rapid drop in the cell performance (named 1st drop), followed by a slow and steady deterioration (named 2nd drop). In the 2nd drop section, the high concentration of H_2S accelerated the voltage loss. While, the voltage drop was not observed at the low H_2S concentration (5ppm). For post-test analyses, X-ray Diffraction Spectroscopy (XRD), scanning electron microscopy (SEM) with energy dispersive X-ray spectroscopy (EDS), and Raman spectroscopy were used. Raman results indicate nickel sulfides were formed in the anode layer, especially at the high H_2S concentration. Thus, the degradation of SOFCs under H_2S containing fuel is attributed to the formation of the nickel sulfide at Ni anode.
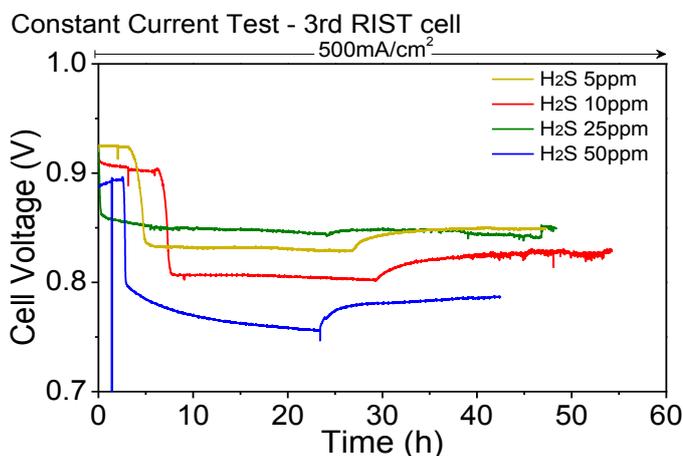
Fig.1 Constant current test with hydrogen sulfide contained fuel respectively 5ppm, 10ppm, 25ppm, and 50ppm at $500mA/cm^2$
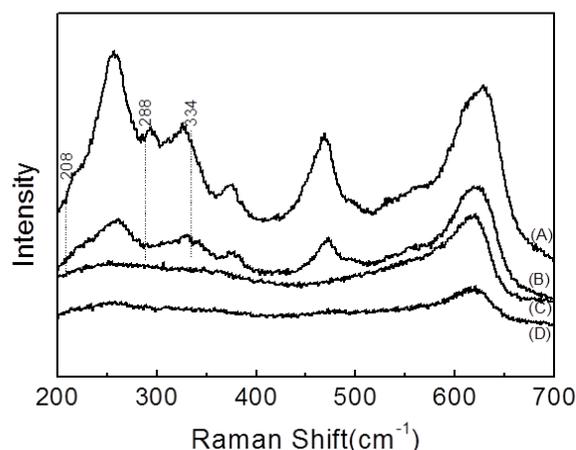
Fig.2 Raman spectra (A) anode(Ni-YSZ cermet) after exposure to H_2 containing 25ppm H_2S, (B) anode(Ni-YSZ cermet) after exposure to H_2 containing 10ppm H_2S, (C) YSZ pellet, and (D) anode(Ni-YSZ cermet)

References
1) T. S. Li, H. Miao, T. Chen, W. G. Wang, and C. Xu, *J. Electrochem. Soc,* **156**, 1383 (2009)
2) B.C.H Steele, A. Heinzel, *Nature*, **414**, 345 (2001)
3) J. Dong, Z. Cheng, S. Zha, M. Liu, *J. Power Sources*, **516**, 461 (2006)

Competition Behavior Between Defect Propagation and Self-Healing under High Temperature Creep in Fiber-Reinforced Self-Healing Ceramics

Jang Won LEE[1], Wataru NAKAO[2]

[1]Graduate School of Engineering, [2]Faculty of Engineering

Yokohama National University, 79-5, Tokiwadai, Hodogayaku, Yokohama 240-8501, Japan
TEL: +81-80-9803-3331   E-mail: Lee-jangwon-dp@ynu.jp

Abstract Fiber-reinforced self-healing ceramics[1] exhibit unique damage tolerance, thereby, anticipated to be next generation structural material, such as turbine blades in jet engine. Its damage tolerance originates from the competition between crack propagation and crack re-bonding due to self-healing. Self-healing function is generated from the high temperature oxidation of healing agent, which is located at the interface between ceramic fiber bundle and matrix, thus, influenced strongly by service temperature. In order to actualize the components made of the fiber-reinforced ceramics, the fracture criteria with the competition is necessary.

Experimental In the present study, the creep fracture behaviour of the fiber-reinforced self-healing ceramics was investigated at high temperatures. From the time change in displacement under tensile stress, the competition behaviour between crack propagation and crack re-bonding was discussed. The used sample is typical fiber-reinforced ceramics, which consists of alumina fiber bundle, alumina matrix and SiC interlayer as healing agent.

Results and Discussion Fig. 1 shows the creep curves of the sample at 1000 $^{\circ}$C. As shown in figure, when tensile stress is 160MPa, the specimen fractured after 6 s. On the other hand, under tensile stress of 137 MPa the creep rate reached to 0 and the specimen could survive for more than 300 h. And, under tensile stress of 150MPa the creep rate reached to 0 and the specimen survived for 1000h. The specimen has cracking strength at 1000 $^{\circ}$C of 47 MPa and final fracture strength of 147 MPa, thus, the creep behaviour was found to include the competition between crack propagation and crack re-bonding due to self-healing. Moreover, creep strength of 137 MPa is quite high, compared to the final fracture strength, therefore, it was found that self-healing function affects the creep strength of self-healing materials strongly.
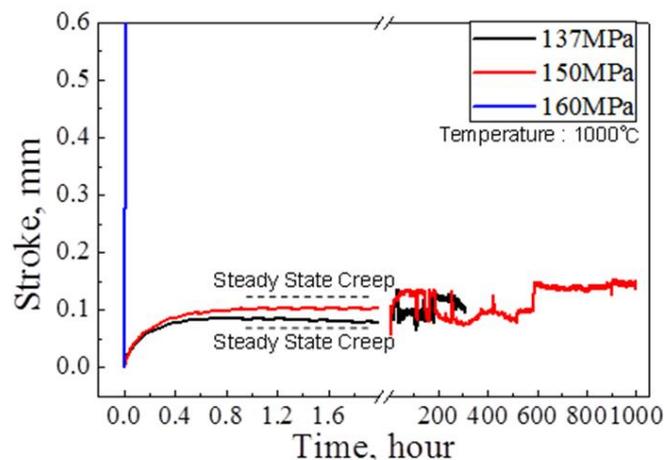
Fig.1 Creep curves of the fiber-reinforced self-healing ceramics at 1000°C

References

1) NAKAO, W, HAGA, Y,: Japanese Patent, 5788309, (2015)

Memo